Available online at www.sciencedirect.com
ScienceDirect
International Journal of Heat and Fluid Flow 28 (2007) 847–861
International Journal of HEAT AND FLUID FLOW
www.elsevier.com/locate/ijhff

Direct numerical simulation of turbulent heat transfer in pipe flows: Effect of Prandtl number

L. Redjem-Saad, M. Ould-Rouiss *, G. Lauriat

LETEM, EA 2546, Université de Marne-la-Vallée, F-77454 Marne-la-Vallée Cedex 2, France

Received 7 February 2006; received in revised form 30 January 2007; accepted 12 February 2007
Available online 6 April 2007

Abstract

Direct numerical simulations of heat transfer in a fully developed turbulent pipe flow with isoflux condition imposed at the wall are performed for a Reynolds number based on pipe radius $Re = 5500$. Main emphasis is placed on Prandtl number effects on turbulent heat transfer in pipe flow. The scaling of mean temperature profiles is investigated in order to derive correct logarithmic law for various Pr. The rms of temperature fluctuations and turbulent heat fluxes are found to increase when increasing Prandtl number. The turbulent Prandtl number, Pr_t, is almost independent of the molecular Prandtl number Pr for $Pr \geqslant 0.2$. The radial distributions of higher order statistics (skewness and flatness) confirm the intermittent behaviour at the close vicinity of the wall; this intermittent behaviour is more pronounced with an increase in Pr. The Nusselt number is in good agreement with the findings of the literature. Probability density functions and joint probability density functions of velocity and temperature fluctuations are used to describe the characteristics of the turbulent flow and heat transfer. The instantaneous flow and thermal fields are plotted in order to analyse the turbulent structures. To explore the impact of the wall curvature on turbulent heat transfer, predictions were compared to available results for channel flow. These comparisons show a slightly more intense temperature fluctuations in the pipe flow.

Keywords: Direct numerical simulation; Prandtl number effect; Turbulent heat transfer; Fully developed pipe flow

1. Introduction

The problem of heat transfer in turbulent pipe flow is of importance in mechanical and engineering fields, and is encountered in a variety of engineering applications. Among these are, for instance, the flow in cooling passages of gas turbine blades, flow in turbomachines, heat exchangers, combustion chambers, nuclear reactors, etc. Many experimental and numerical studies of heat transfer in fully developed turbulent pipe flow have been performed during the past decades. Most of the earlier research works were based on the analogy between fluid friction and heat transfer, and turbulent heat transfer was examined by postulating that the laws governing momentum and heat transfer are similar (Von Karman, 1939; Martinelli, 1947).

Some measurements have been made to determine the Prandtl number effects in turbulent pipe flow. Gowen and Smith (1967) presented results of a systematic study of the Prandtl effects over the range $0.026 \leqslant Pr \leqslant 14.3$ on temperature profiles, for turbulent flows in a smooth tube for the Reynolds number range $[10^4–5 \times 10^4]$. These profiles were represented by the universal distribution:

$$T^+ = A_s \ln y^+ + B_s \quad \text{where } B_s = 5 \ln \frac{5Pr + 1}{30} + 8.55 + 5Pr$$

The authors concluded that the value of constant A_s appears to be relatively insensitive to Prandtl and Reynolds numbers.

The equations derived by Kader (1981) are based on interpolation arguments and permit evaluation of the temperature profiles in a turbulent tube flow at many values of Prandtl number (or in plane channel, or in a boundary layer above a smooth plane). It was shown that the predicted

* Corresponding author.
E-mail address: ould@univ-mlv.fr (M. Ould-Rouiss).

0142-727X/$ - see front matter © 2007 Elsevier Inc. All rights reserved.
doi:10.1016/j.ijheatfluidflow.2007.02.003

Nomenclature

D	pipe diameter
$F(\Theta')$	flatness of temperature fluctuations
h	heat transfer coefficient
k	thermal conductivity
L	length of the computational domain
Nu	Nusselt number, $Nu = hD/k$
Pr	Prandtl number, $Pr = \nu/\alpha$
Re	Reynolds number $Re = U_p R/\nu$
r	dimensionless coordinate in radial direction scaled by the pipe radius
R	pipe radius
$S(\Theta')$	skewness of temperature fluctuations
T	temperature
T_b	bulk temperature
T_r	reference temperature, $T_r = q_w/\rho C_p U_b$
T_w	wall temperature
T_τ	friction temperature, $T_\tau = q_w/\rho C_p u_\tau$
u_τ	friction velocity
U_b	bulk velocity
U_p	centreline streamwise velocity of the laminar Poiseuille flow
y^+	distance from the wall in viscous wall units, $y^+ = (R - r)u_\tau/\nu$
z	coordinate in axial direction

Greeks

θ	coordinate in circumferential direction
Θ	dimensionless temperature, $\Theta = (\langle T_w \rangle - T)/T_r$
ν	kinematic viscosity

Superscripts

$\overline{(\cdot)}$	statistically averaged
$(\cdot)^+$	normalized by u_τ, ν and T_τ
$\langle\cdot\rangle$	averaged over the pipe section
$(\cdot)'$	fluctuation component

temperature distributions are in quite satisfactory agreement with experimental data. Yakhot et al. (1987) used an expression for the turbulent Prandtl number (Pr_t) obtained from the renormalization group procedure to describe heat transfer in turbulent pipe flow. They showed that the proposed relation between turbulent viscosity and turbulent diffusivity gives accurate predictions for Nusselt number and temperature distributions in wide ranges of Prandtl and Reynolds numbers ($1 < Pr < 10^6$ and $2.5 \times 10^4 < Re < 2 \times 10^5$).

There is an extensive litterature on heat transfer coefficients in pipes (Petukhov, 1970; Kays and Perkins, 1973; Sleicher and Rouse, 1975; Musschenga et al., 1992; Tricoli, 1999). These investigations provide correlations for predicting heat transfer for constant and variable property fluids. Tricoli (1999) indicated that over several decades, two approaches have been widely used to model heat transfer at wall boundary: the eddy diffusivity model and the surface renewal model (Musschenga et al., 1992). He pointed out that the concepts and quantities involved in these models have no well-based relationships with the correlated turbulent fluctuations which are the fundamental quantities underlying turbulent transport. Thus a rational approach to transport in turbulent flow must be based on turbulence fluctuations as well as on molecular viscosity, heat or mass diffusivity. The analysis of Tricolli, which was derived from these first principles, gives a new analogy between heat and momentum transport in turbulent incompressible pipe flow (and arbitrary shaped duct), for $Pr \ll 1$. The analogy could be used to infer correlations for heat transfer in some systems with complex geometry, just from pressure drop measurements.

Accurate predictions of the flow field in the near wall region being a prerequisite for correct predictions of the heat transfer rate, low Reynolds-number models could lead to good agreements with experimental data when RANS-approaches are used. The most frequently adopted models are the $k - \epsilon$ models (Myong et al., 1989; Takagi and Hirai, 1998, Thakre and Joshi, 2000). Twelve versions of low Reynolds $k - \epsilon$ models and two low Reynolds number for Reynolds stress turbulence models were analyzed by Thakre and Joshi (2000). The heat transfer predictions were compared with the experimental data of Gowen and Smith (1967), Kader (1981), Bremhorst and Bullock (1973) and Hishida et al. (1986). Thakre and Joshi (2000) showed that the $k - \epsilon$ models performed relatively better than the Reynolds stress models for predicting the mean axial temperature and the Nusselt number in pipe flows, for different Prandtl numbers. They concluded that the predictive ability of the $k - \epsilon$ models is expected to improve when turbulent Prandtl number variations near the wall are included. The authors pointed out that the overall discrepancy observed in both the $k - \epsilon$ and the RSM models for heat transfer can be attributed to the incorrect near-wall modeling of the dissipation term. They pointed out also the lack of detailed near-wall temperature and scalar flux measurements at higher Prandtl numbers.

In view of the above literature review, it clearly appears a need of quantitatively credible information on heat and momentum transport near the wall. Experiments which reveal the mechanistic picture of heat and momentum in the wall region are only few, owing to the difficulty in measuring the Reynolds stress and turbulent heat flux fluctuations very close to the wall. Hishida et al. (1986) have developed techniques for turbulence measurements near the wall with specially devised, symmetrically bent V-shaped hot-wires, and investigated the structural similarity between momentum and heat transfer. The transport of

heat and momentum near the wall was found to be very intermittent and strongly associated with the coherent turbulent structures. The profiles of turbulence energy components, temperature variance, Reynolds shear stress and turbulent heat fluxes were well displayed in the wall region so that the measurements are useful to assess currently used models and for new developments.

With the advent of supercomputers, direct numerical simulation (DNS) offers valuable data for turbulent heat transfer. The literature survey reveals that most DNS studies have been performed for channel and annulus flows and that DNS of heat transfer in turbulent pipe flows are very scarce. DNS of turbulent heat transfer in fully developed pipe flow was performed by Satake and Kunugi (2002) and by Piller (2005) for only one Prandtl number ($Pr = 0.71$). Many attempts have been made to explore the effect of Pr on turbulent heat transfer in channel flows with DNS (Kawamura et al., 1998, 1999; Na and Hanratty, 2000). To our best knowledge, there is no DNS of turbulent heat transfer in pipe flows at various Prandtl numbers. The present work is the first DNS which investigate the effects of low to intermediate Pr on turbulent heat transfer in pipe flows under isoflux wall condition. Turbulent thermal statistics and wall thermal behaviour are analyzed and compared with published experimental and numerical results. The DNS predictions are also compared to those obtained in the channel flow.

2. Governing equations and numerical procedure

The flow configuration investigated is a forced, fully developed, incompressible pipe flow of a Newtonian fluid heated with a uniform heat flux q_w imposed at the wall (Fig. 1). The fluid properties are assumed constant and the viscous dissipation term is neglected. Therefore, temperature may be considered as a passive scalar. The dimensionless temperature Θ is defined as:

$$\Theta = (\langle T_w \rangle - T)/T_r \tag{1}$$

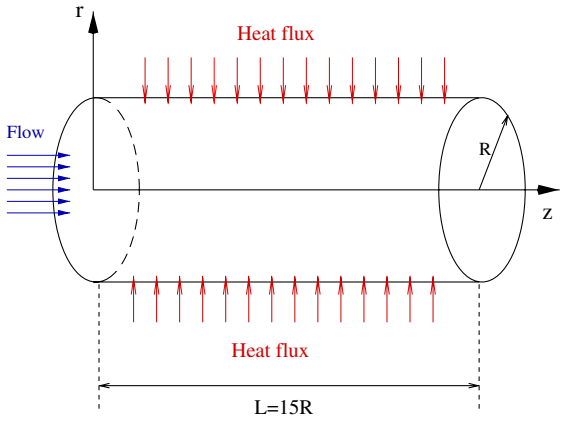

Fig. 1. Schematic of the computational domain.

where $T_r = q_w/\rho C_p U_b$ is the reference temperature and $\langle T_w \rangle$ denotes the wall temperature averaged in time and circumferencial direction. Using the dimensionless variables $q_r = r \cdot v_r$, $q_\theta = r \cdot v_\theta$, $q_z = v_z$, the energy equation writes as follow:

$$\frac{\partial \Theta}{\partial t} + \frac{1}{r}\frac{\partial}{\partial r}(q_r \Theta) + \frac{1}{r}\frac{\partial}{\partial \theta}(q_\theta \Theta) + \frac{\partial}{\partial z}(q_z \Theta) - q_z \frac{1}{T_r}\frac{\partial \langle T_w \rangle}{\partial z} = \frac{1}{Re\,Pr}\left[\frac{1}{r}\frac{\partial}{\partial r}\left(r\frac{\partial \Theta}{\partial r}\right) + \frac{1}{r^2}\frac{\partial^2 \Theta}{\partial \theta^2} + \frac{\partial^2 \Theta}{\partial z^2}\right] \tag{2}$$

where r and the velocity components are scaled by the pipe radius R and the centreline streamwise velocity of the laminar Poiseuille profile U_p, respectively. The Reynolds number Re is defined as $Re = U_p R/\nu$.

The heating condition imposed on the wall implies a linear increase of the bulk temperature $\langle T_b \rangle$ in the streamwise direction. For fully developed flows, the following equalities are satisfied:

$$\frac{\partial \langle T \rangle}{\partial z} = \frac{\partial \langle T_b \rangle}{\partial z} = \frac{\partial \langle T_w \rangle}{\partial z} = \frac{2 q_w}{\rho C_p U_b} = 2 T_r \tag{3}$$

The wall temperature fluctuations are assumed to be zero and the dimensionless temperature boundary condition is $\Theta = 0$. This condition corresponds to the mixed-type boundary condition described by Piller (2005). In this case, the time-averaged wall heat flux is uniform in space, and the wall temperature is not time-dependent and varies linearly along the streamwise direction.

The governing equations were discretized on a staggered mesh in cylindrical coordinates with a computational length in the axial direction $L = 15R$. The numerical integration was performed by a finite difference scheme, second-order accurate in space and in time. The time advancement employed a fractional step method. A third-order Runge–Kutta explicit scheme and a Crank–Nicolson implicit scheme were used to evaluate the convective and diffusive terms, respectively. Uniform computational grid and periodic boundary conditions were applied to the circumferential and axial directions. In the radial direction, non-uniform meshes specified by hyperbolic tangent functions were employed. The momentum and continuity equations were solved as described in the paper by Feiz et al. (2005). Computations were carried out on $(N_\theta \times N_r \times N_z) = (129 \times 95 \times 129)$ grid for $Pr = 0.026$ and $(N_\theta \times N_r \times N_z) = (129 \times 129 \times 257)$ grid for higher Prandtl numbers, corresponding to the spatial resolution $(R\Delta\theta^+, \Delta r^+, \Delta z^+) = (10, 0.01\text{–}7, 20)$ and $(R\Delta\theta^+, \Delta r^+, \Delta z^+) = (10, 0.01\text{–}5, 10)$, respectively. The turbulent heat transfer was solved with the same grid points than fluid turbulence. Indeed the thickness of the conduction region, δ_T, depends on the Pr value: for $Pr < 1$ the ratio of the thermal boundary layer to the dynamic boundary layer varies as $\delta_T/\delta_U = Pr^{-1/2}$ while it varies as $\delta_T/\delta_U = Pr^{-1/3}$ for $Pr > 1$. Consequently, for high Prandtl numbers, the grid resolution which captures the viscous sublayer can be inadequate and insufficient for the thermal conduction region. For small

Prandtl numbers, the opposite behaviour is observed (Montreuil, 2000). Owing to the grid requirement, the DNS of turbulent heat transfer becomes thus much difficult to handle for $Pr \gg 1$. Since the present DNS of turbulent heat transfer are conducted for $Pr \leqslant 1$, less grid resolution is required. Consequently, we ran DNS on a grid mesh finer than the one required for fully developed turbulent flow and adequate for turbulent heat transfer, with care taken so that the computational domain is enlarged to capture larger thermal scales. Moreover, the above grids were found to provide an accurate prediction of turbulence statistics (in agreement with the available data of the literature) and to give a good compromise between the required CPU-time and accuracy. It is also noted that the streamwise spectra of temperature near the wall ($y^+ = 5$) for different Pr, drop several orders of magnitude without energy accumulation at high wave numbers. The two-point correlations of fluctuating streamwise velocity and temperature fall off to zero when the separation approaches half the pipe length. These observations indicate an adequate spatial resolution of the present simulations.

3. Results and discussion

3.1. Mean velocity profile and root mean square

The streamwise mean velocity profile is plotted in Fig. 2 versus the distance from the wall in wall units at $Re = 5500$ ($Re_\tau = 186$). The viscous sublayer and the buffer region are well resolved in the present DNS. The predicted profile coincides with the numerical data by Eggels et al. (1994) obtained in a pipe flow. In the logarithmic region, far from the wall, the agreement with the universal logarithmic law is not good for the present DNS as well as for Eggel et al. data, because of the small value of Reynolds number.

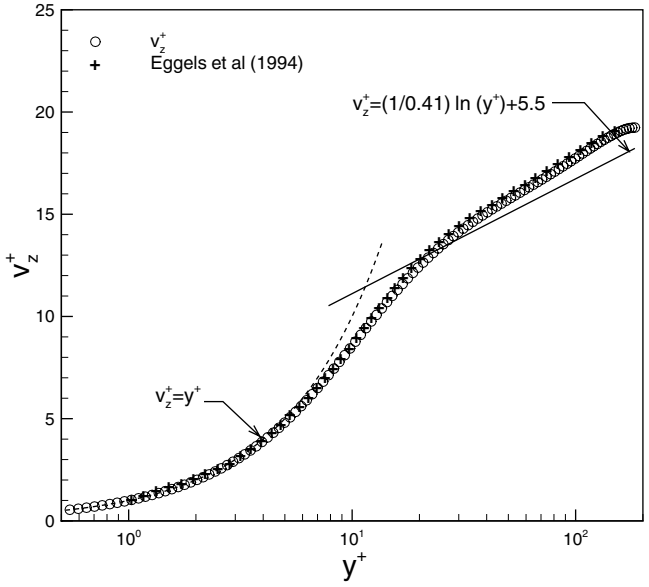

Fig. 2. Mean velocity profile ($Re = 5500$).

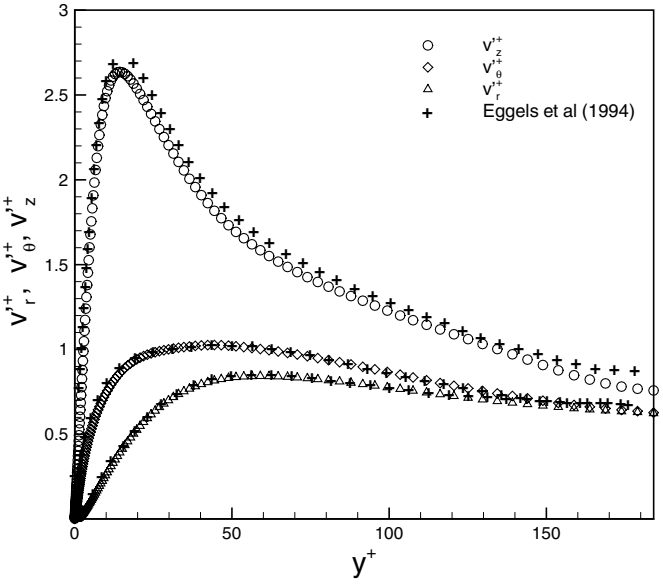

Fig. 3. RMS of velocities fluctuations ($Re = 5500$).

Indeed, the logarithmic law is only justified at large Re (Tennekes and Lumley, 1972). The friction factor ($C_f = 9.25 \times 10^{-3}$) is in good agreement with the DNS results reported by Eggels et al. (1994) ($C_f = 9.22 \times 10^{-3}$) and Piller (2005) ($C_f = 9.32 \times 10^{-3}$). Fig. 3 illustrates the root mean square (rms) of velocity fluctuations as a function of y^+ ($(y^+ = u_\tau y/\nu)$). They are compared to the data by Eggels et al. (1994) obtained at ($Re_\tau = 180$). The overall agreement between present predictions and those obtained by Eggels et al. is satisfactory. The present DNS, however, underpredicts slightly the rms of streamwise velocity fluctuations.

3.2. Mean temperature profiles

The dimensionless mean temperature distributions normalized by the friction temperature ($T_\tau = q_w/\rho C_p u_\tau$) are shown in Fig. 4a as a function of the wall distance for various Prandtl numbers at $Re = 5500$. The predicted profile for $Pr = 0.71$ is in good agreement with Satake and Kunugi (2002) who performed DNS of turbulent heat transfer in pipe air flow at $Re = 5283$. The temperature profile for the highest Prandtl number considered ($Pr = 1$) reveals that the thermal resistance is mainly concentrated in the conductive sublayer which is immersed in the viscous sublayer. Beyond the conductive sublayer there is a rapid transport of heat in the pipe. When the Prandtl number decreases, the conductive sublayer spreeds from the wall to the core region. The temperature profile for the smallest Prandtl number ($Pr = 0.026$) indicates that the molecular heat transfer dominates.

It should be noted that the logarithmic region can be better distinguished from the buffer region when the Prandtl number increases. For small Prandtl numbers, the logarithmic part of the temperature profile appears only at

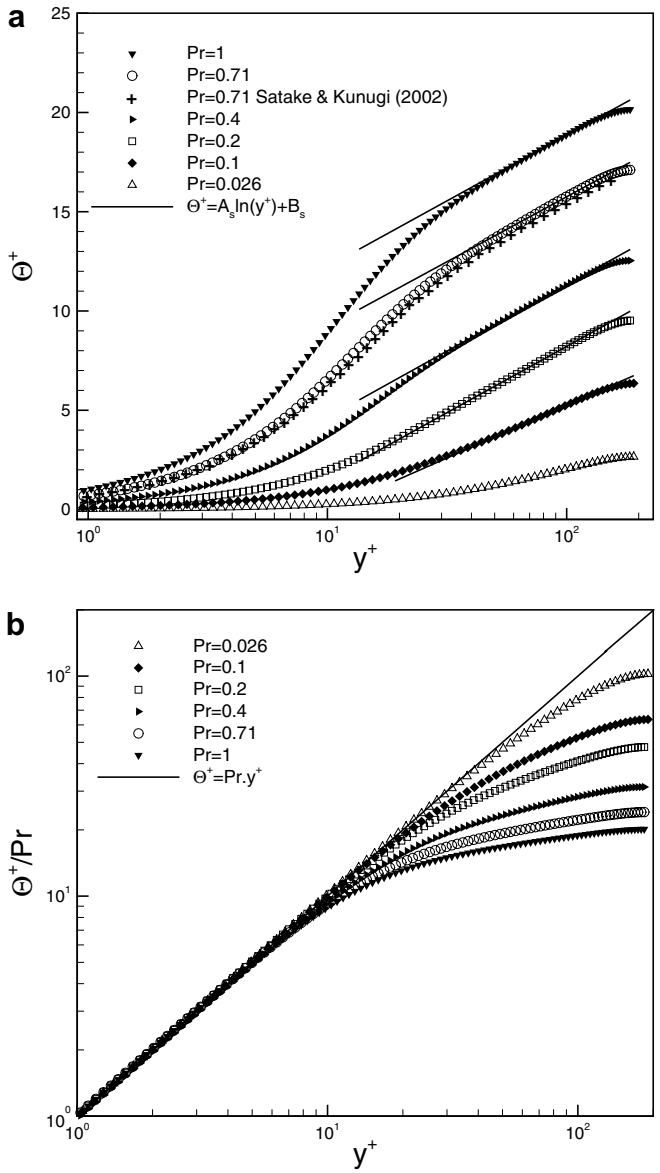

Fig. 4. Mean temperature profile ($Re = 5500$).

high Reynolds numbers ($Re > 10^5$). It is generally reported that the temperature profile in the vicinity of the wall can be expanded as $\Theta^+ = Pry^+ + \cdots$. Fig. 4b displays clearly such an asymptotic behaviour, within the near wall region, and confirms that the conductive sublayer is deeply immersed in the viscous sublayer for small Prandtl numbers.

3.3. Scaling of the mean temperature profile

Written in terms of the inner variables, the logarithmic law for the mean temperature distribution reads:

$$\Theta^+ = \frac{1}{\kappa_\Theta} \ln y^+ + \beta_\Theta$$

where the von Karman constant of mean temperature distribution, κ_Θ, is usually assumed independent of Prandtl and Reynolds numbers. Direct numerical simulations allow an accurate determination of the quantities κ_Θ and β_Θ in the logarithmic region. To provide a correct value for these constants, it is useful to consider the relationship:

$$\kappa_\Theta = \frac{1}{y^+}\left(\frac{\mathrm{d}\Theta^+}{\mathrm{d}y^+}\right)^{-1} \tag{4}$$

and, just replacing it in the logarithmic law, one can obtain the value of the β_Θ from

$$\beta_\Theta = \Theta^+ - \frac{1}{\kappa_\Theta} \ln y^+ \tag{5}$$

Fig. 5a and b gives the distribution of κ_Θ and β_Θ for various Pr. These quantities have to be constant in the logarithmic region. For the smallest Prandtl numbers, the plateau in κ_Θ is not observed, probably due to the low Re considered. For higher Prandtl numbers ($Pr > 0.2$), κ_Θ

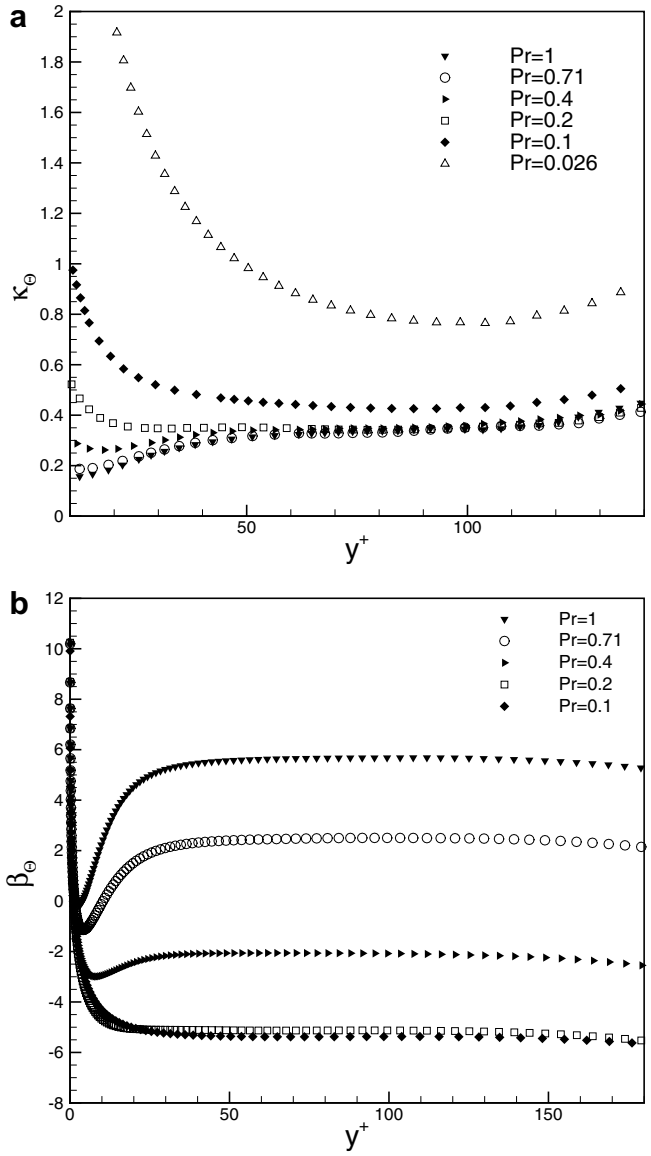

Fig. 5. Scaling of mean temperature profile.

exhibits a plateau. It is also clear that the extend of the logarithmic region becomes smaller as Pr decreases. The plateau value of $\kappa_\Theta = 0.347$ agree well with Piller's result for $Pr = 0.71$ ($\kappa_\Theta = 0.34$) and is smaller than the DNS prediction by Kawamura et al. (1999) in channel flow ($\kappa_\Theta \simeq 0.4$). From Fig. 5a, no Prandtl number dependence is evidenced for $Pr \geqslant 0.2$. This is not seen in the distribution of β_Θ. Fig. 5b shows that β_Θ increases with increases in Pr. Therefore, the Prandtl number affects the value of β_Θ more than that of κ_Θ.

3.4. RMS of temperature fluctuations

The rms-distribution of temperature fluctuations normalized by the friction temperature is shown in Fig. 6a. For comparison purpose, the results by Satake and Kunugi (2002) for $Pr = 0.71$ are also included. The present DNS is in good agreement with their results and the maximum of temperature fluctuations is also located at $y^+ \simeq 18$. When the Prandtl number increases, the peak of the temperature fluctuations moves towards the wall and a noticeable rise in this peak can be observed. For $Pr = 1$, the peak is located at $y^+ \simeq 16$. Note that the maximum of the rms temperature fluctuations is close to the maximum of rms of streamwise velocity fluctuations $y^+ \simeq 14$. When $Pr = 0.026$ the conductive sublayer dominates, the peak of temperature fluctuations being located at $y^+ \simeq 78$.

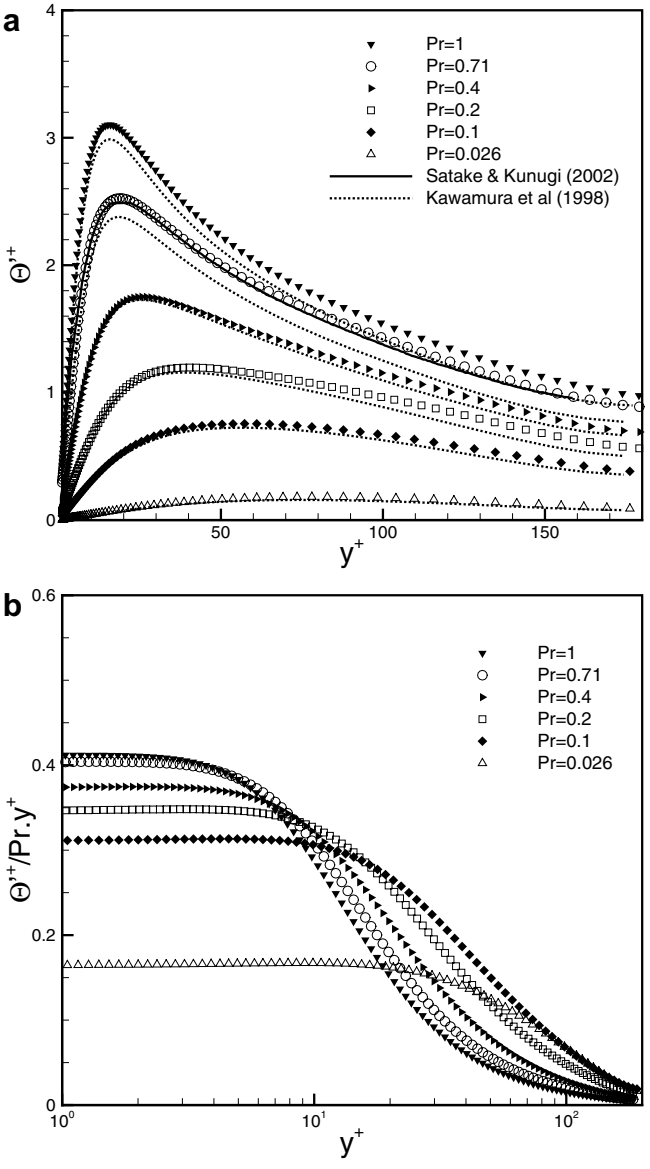

Fig. 6. RMS of temperature fluctuations ($Re = 5500$).

The rms temperature fluctuations are compared with the previous results obtained by Kawamura et al. (1998) in channel flow for $Re_\tau = 180$. There is a good agreement with the DNS data of Kawamura et al. at wall distances y^+ smaller than a certain value y_1^+ (Fig. 6a). For $Pr = 0.71$, we found $y_1^+ \simeq 20$, in accordance with Piller's estimation. With a decrease in Pr, y_1^+ shifts towards the pipe axis. At $y^+ > y_1^+$, the present DNS is slightly larger than the rms temperature fluctuations of the channel flow, supporting thus Piller's (2005) observation for $Pr = 0.71$.

The temperature fluctuations Θ'^+ can be expanded in the immediate vicinity of the wall as:

$$\Theta'^+ = Pr(b_\Theta y^+ + c_\Theta y^{+2} + \cdots) \tag{6}$$

where b_Θ is a function of Prandtl number which decreases with Pr. As the wall is approached, the evolution of the rms temperature fluctuations confirms the asymptotic behaviour $\Theta'^+ \simeq b_\Theta Pr y^+$, as it can be seen in Fig. 6b. It appears also that the coefficient b_Θ becomes independent of Pr for the highest values of Pr considered here. These trends confirm the Kawamura et al. (1998) predictions for channel flows. The asymptotic value of b_Θ (i.e. the wall value) is about 0.4 for $Pr = 0.71$ which is slightly larger than the predicted value of Kawamura et al. (1999) in channel flow ($b_\Theta \simeq 0.38$). This discrepancy may be due to the difference in the Re-values as well as in the wall curvature effect. However, for the smallest Prandtl number ($Pr = 0.026$), the wall value which is about 0.16 agrees well with the result of Kawamura et al. (1999).

3.5. Turbulent heat fluxes

The streamwise turbulent heat flux normalized by the friction velocity and temperature is reported in Fig. 7a for different Prandtl numbers. The agreement between the predicted streamwise turbulent heat flux at $Pr = 0.71$ and the one by Satake and Kunugi (2002) is remarquably good.

For $Pr = 0.71$, the maximum in the streamwise turbulent heat flux occurs at $y^+ \simeq 16$. This value is located between the maximum of rms streamwise velocity fluctuations ($y^+ \simeq 14$) and the maximum of rms temperature fluctuations ($y^+ \simeq 18$). Similar observation has been found in the DNS of heat transfer in turbulent channel flow by Kawamura et al. (1998). Fig. 7a indicates that, irrespective of the Prandtl number, the flow geometry has practically no effect on the streamwise turbulent heat flux. The behaviour of the peak in the streamwise turbulent heat flux is

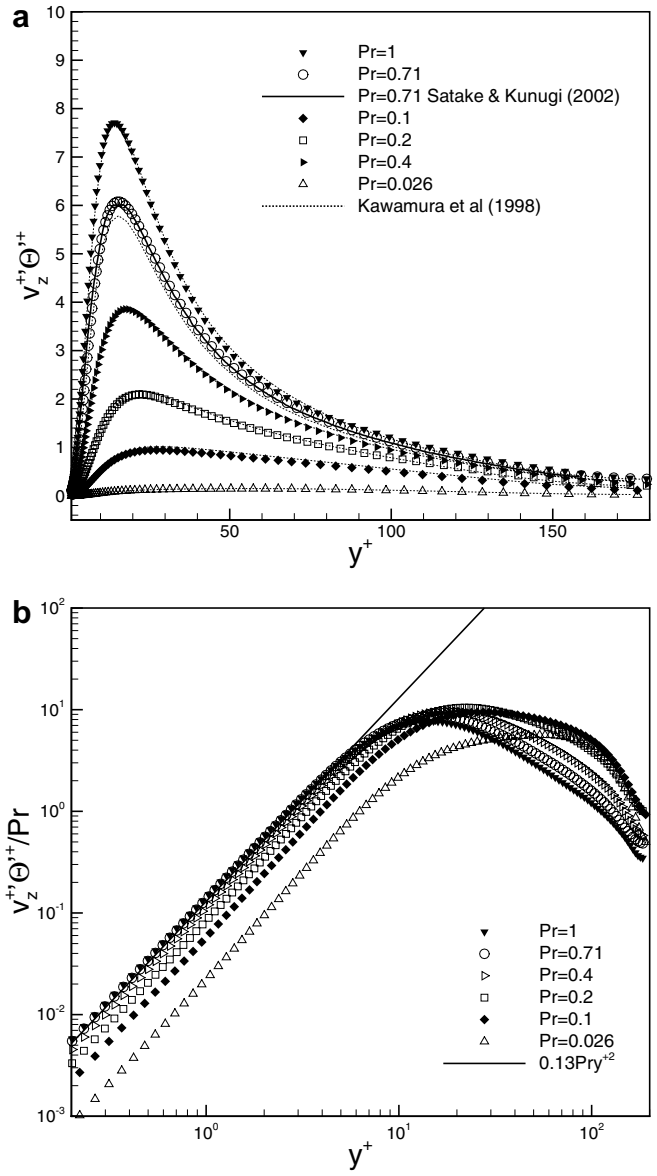

Fig. 7. Streamwise turbulent heat flux ($Re = 5500$).

similar to that of the rms temperature fluctuations: when the Prandtl number increases, the conductive sublayer becomes thinner and the peak value in the streamwise turbulent heat flux increases and shifts towards the wall. The position of the peak moves from $y^+ \simeq 57$ for $Pr = 0.026$ to $y^+ \simeq 22$ for $Pr = 0.2$, and $y^+ \simeq 14$ for $Pr = 1$.

To analyze the near-wall asymptotic behaviour of the turbulent thermal statistics, the velocity fluctuations can be expanded in terms of y^+ as follows:

$$v_z'^{+} = b_z y^{+} + c_z y^{+2} + \cdots \tag{7}$$

$$v_r'^{+} = b_r y^{+2} + c_r y^{+3} + \cdots \tag{8}$$

Considering the expansions of the temperature and velocity fluctuations, the turbulent streamwise heat flux is given by:

$$\overline{v_z'^{+}\Theta'^{+}} = Pr\left(\overline{b_z b_\Theta} y^{+2} + \overline{c_z b_\Theta} y^{+3} + \cdots\right) \tag{9}$$

which indicates that, in the vicinity of the wall, the axial turbulent heat flux varies as:

$$\overline{v_z'^{+}\Theta'^{+}}/Pr \simeq \overline{b_z b_\Theta} y^{+2}, \quad y^{+} \to 0 \tag{10}$$

Fig. 7b displays clearly this asymptotic behaviour when the wall is approached, with $\overline{b_z b_\Theta} \simeq 0.13$ for $Pr = 0.71$ and $Pr = 1$. This predicted $\overline{b_z b_\Theta}$ is consistent with the one in channel flow ($\overline{b_z b_\Theta} \simeq 0.12$, Kawamura et al., 1998). The value of the coefficient $\overline{b_z b_\Theta}$ is reduced for $Pr = 0.026$ because b_Θ decreases. These results confirm that the coefficient b_Θ is almost independent of Pr when $Pr > 0.2$.

The profile of the wall-normal turbulent heat flux is plotted in Fig. 8a for different Prandtl numbers. In comparison to the streamwise turbulent heat flux, the wall-normal heat flux is smaller and reaches a maximum farther away from the wall. The present DNS is in close agreement with

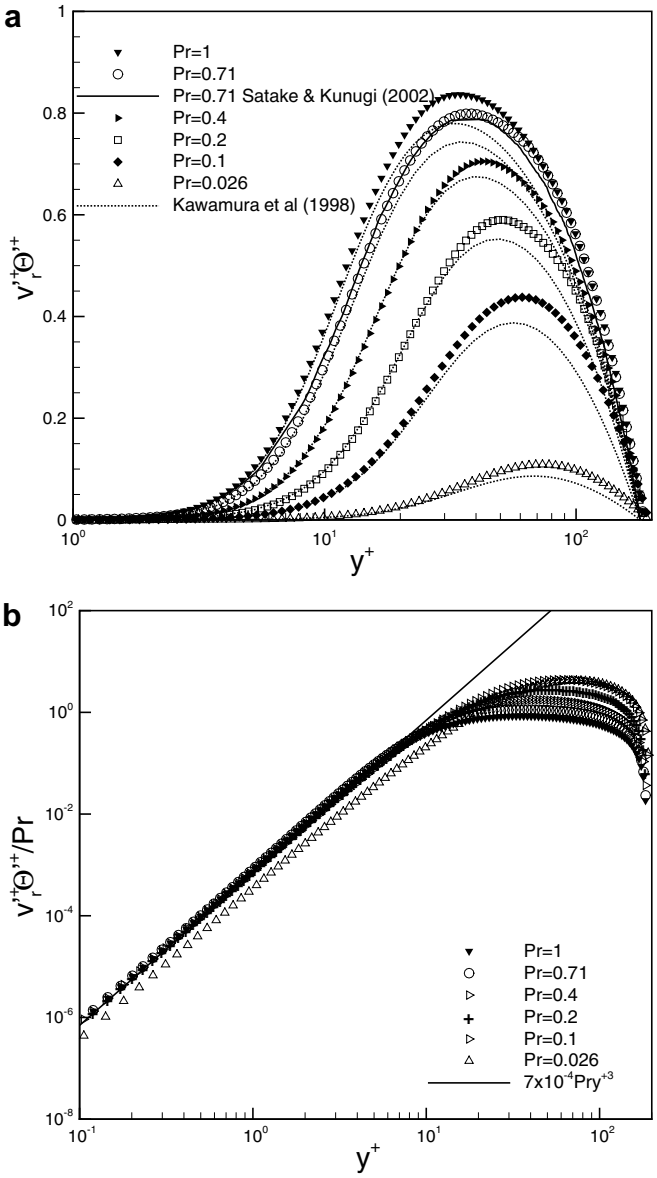

Fig. 8. Wall-normal turbulent heat flux ($Re = 5500$).

the wall-normal heat flux of Satake and Kunugi (2002). Fig. 8a reveals that, irrespective of Pr number, the radial turbulent heat flux is affected by the duct curvature. The radial turbulent heat flux in the pipe is more important than in channel flow. This supports Piller's conclusion. Moreover, the distributions of the radial turbulent heat flux and total heat flux are curvilinear as in the case of total shear stress in Feiz et al. (2005).

The total heat flux, sum of the conductive (molecular) heat flux and turbulent heat flux, is given by:

$$q_{\text{total}} = \frac{1}{Pr}\frac{\mathrm{d}\Theta^+}{\mathrm{d}y^+} - \overline{v_{\mathrm{r}}'^+\Theta'^+} \tag{11}$$

When the Prandtl number increases, the radial turbulent heat flux increases. It is balanced by the decrease in the conductive heat flux. The peak of the wall-normal turbulent heat flux increases and moves towards the wall, from $y^+ \simeq 55$ for $Pr = 0.026$, to $y^+ \simeq 40$ for $Pr = 0.71$, and $y^+ \simeq 35$ for $Pr = 1$. Our predictions agree with the asymptotic behaviour of the turbulent wall-normal heat flux:

$$\overline{v_{\mathrm{r}}'^+\Theta'^+} = Pr\left(\overline{c_{\mathrm{r}}b_\Theta}y^{+3} + \overline{d_{\mathrm{r}}b_\Theta}y^{+4} + \cdots\right) \tag{12}$$

which indicates that, in the vicinity of the wall, the radial turbulent heat flux varies as:

$$\overline{v_{\mathrm{r}}'^+\Theta'^+}/Pr \simeq \overline{c_{\mathrm{r}}b_\Theta}Pry^{+3}, \quad y^+ \to 0 \tag{13}$$

For highest values of Pr, the distributions of the wall-normal heat flux develops as y^{+3} up to $y^+ \simeq 6$ and tends to zero when approaching the wall (Fig. 8b). It is, however, relevant to note that the coefficient $\overline{c_{\mathrm{r}}b_\Theta}$ is almost independent of Pr for $Pr \geqslant 0.2$. Its value is about $\overline{c_{\mathrm{r}}b_\Theta} \simeq 7 \times 10^{-4}$ and confirms the Kawamura et al. (1998) results for a channel flow. Note that Chapman and Kuhn (1986) found that this asymptotic behaviour is valid up to $y^+ \simeq 3$. Myong et al. (1989) showed that the y^{+3} behaviour near the wall holds up to $y^+ \simeq 5$ and that the coefficient $\overline{c_{\mathrm{r}}b_\Theta}$ varies between 5×10^{-4} and 7×10^{-4}.

3.6. Cross-correlation coefficients

For $Pr = 0.71$, the cross-correlation coefficient of the streamwise turbulent heat flux, $R_{v_z\Theta}$, is larger than the cross-correlation coefficient of the wall-normal turbulent heat flux, $R_{v_{\mathrm{r}}\Theta}$, throughout the pipe section as it can be seen in Fig. 9a and b. This result means that the temperature fluctuations are better correlated with streamwise velocity fluctuations than the transverse ones. The maximum value reached by the coefficient $R_{v_z\Theta}$ ($\simeq$0.95) is almost twice the one reached by the coefficient $R_{v_{\mathrm{r}}\Theta}$, ($\simeq$0.5), confirming that the streamwise turbulent heat flux reaches much larger values than the wall-normal heat flux. These trends agree well with those of Kawamura et al. (1999) and Piller (2005) for $Pr = 0.71$. When Pr is close to unity, the Reynolds shear stress coefficient $R_{v_{\mathrm{r}}v_z}$ coincides with the coefficient $R_{v_{\mathrm{r}}\Theta}$. Far from the wall, $R_{v_{\mathrm{r}}\Theta}$ decreases significantly with an increase in Pr (Fig. 9a) while $R_{v_z\Theta}$ presents a completely different trend when Pr increases. The coefficient $R_{v_z\Theta}$ increases if Pr is smaller than unity. The predicted $R_{v_{\mathrm{r}}\Theta}$ agree well with Piller's DNS for $30 \leqslant y^+ \leqslant 70$ (plateau), and is slightly larger for the other wall distances. The predicted $R_{v_z\Theta}$ is also in fair agreement with Piller's result. The wall values of $R_{v_z\Theta}$ compare fairly well with those for channel flow (Kawamura et al., 1999) at various Pr: $R_{v_z\Theta} \simeq 0.34$ for $Pr = 0.026$, $R_{v_z\Theta} \simeq 0.65$ for $Pr = 0.2$ and $R_{v_z\Theta} \simeq 0.95$ for $Pr = 0.71$.

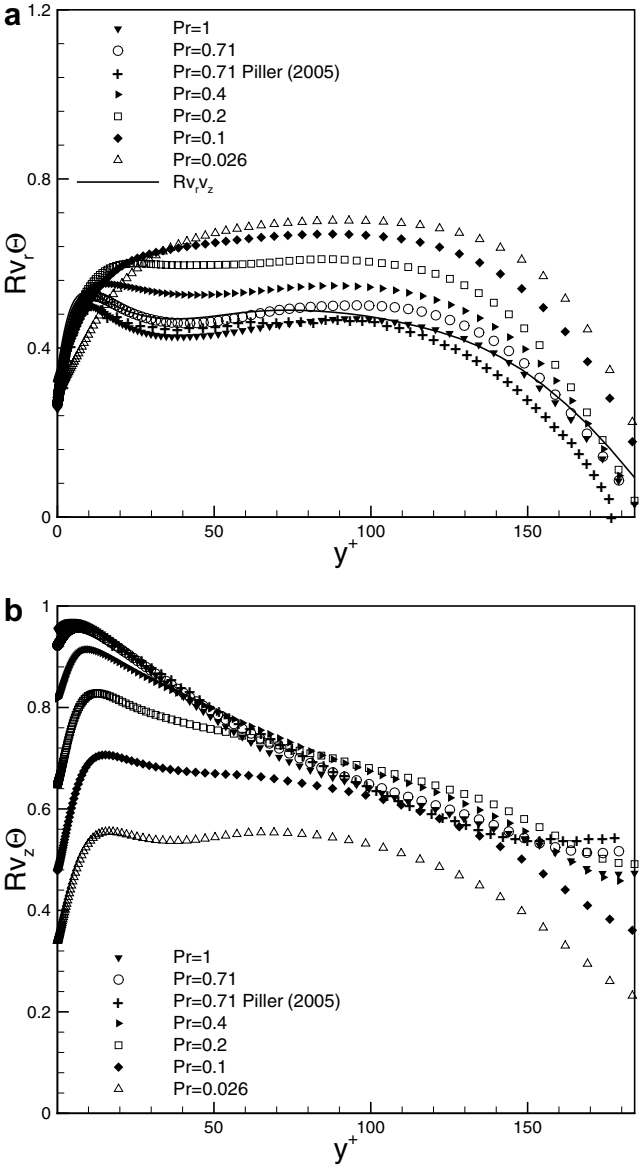

Fig. 9. Cross-correlation coefficients: (a) $R_{v_{\mathrm{r}}\Theta}$ and (b) $R_{v_z\Theta}$.

3.7. Turbulent Prandtl number

The knowledge of Pr_{t} is used to predict heat transfer (thermal field) from known velocity field, and particularly in the near-wall region where the profile of Pr_{t} has been a matter of conjuncture. In Fig. 10, the results of Piller are included for comparison. The present predictions for

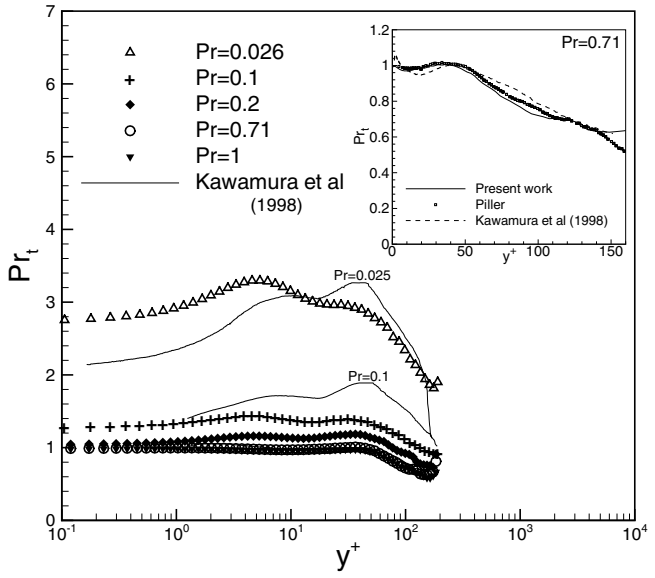

Fig. 10. Turbulent Prandtl number.

$Pr = 0.71$ coincide well with the results of Piller, although there is a slight discrepancy far away from the wall. The best agreement is obtained near the wall. In the near-wall region, Pr_t is consistent with the well known limiting behaviour for $Pr \geqslant 0.2$ and reaches a value from about $Pr_t = 0.98$. For $Pr < 0.2$, the turbulent Prandtl number increases ($Pr_t \simeq 1.4$ for $Pr = 0.1$, $Pr_t \simeq 2.7$ for $Pr = 0.026$). Far from the wall $y^+ > 50$, Pr_t decreases. These trends indicate that near the wall, the momentum diffusion is much larger than heat diffusion.

For $Pr \geqslant 0.2$, the influence of the flow geometry on Pr_t is quite small. However, for smaller Pr, the turbulent Prandtl number is noticeably affected by the flow geometry, suggesting that the wall curvature has a significant influence on turbulent heat transfer. The influence of Pr on Pr_t is more pronounced with decreasing Prandtl number, in accordance with the values of Nusselt number (Table 1) which indicates larger differences between Nu in pipe and Nu in channel as Pr decreases. The present predictions agree well with the wall values of Kawamura et al. (1998) for $Pr \geqslant 0.2$. It should be noted that the asymptotic behaviour of Pr_t, as approaching the wall, is practically insensitive to the molecular Prandtl number for $Pr \geqslant 0.2$, which shows that Pr_t is independent of Pr, as reviewed by Kawamura et al. (1998) and Myong et al. (1989). This also supports the usual assumption of a constant Pr_t in many engineering calculations (for $Pr \geqslant 0.2$).

Table 1
Nusselt number for various Prandtl numbers

Pr	Pipe				Channel
	Present	Gnielinski (1976)	Piller (2005)	Sleicher and Rouse (1975)	Kawamura et al. (1998)
0.026	6.78	–	–	5.82	5.4 ($Pr = 0.025$)
0.1	9.43	–	–	7.82	–
0.2	11.4	–	–	10.22	10.32
0.4	15.28	–	–	14.75	14.18
0.71	19.36	18.17	18.54	20.32	18
1	22.3	21.06	–	24.72	–

3.8. Higher-order statistics

Indications of the intermittent character of the wall region are high-order statistics such as skewness and flatness. Fig. 11 display the radial distributions of skewness ($S(\Theta') = \langle\Theta'^3\rangle/\langle\Theta'^2\rangle^{\frac{3}{2}}$) and flatness ($F(\Theta') = \langle\Theta'^4\rangle/\langle\Theta'^2\rangle^2$) coefficients, respectively, for various Prandtl numbers. For $Pr = 0.026$, the skewness of the temperature fluctuations is about 0.8. For higher Prandtl numbers, the skewness grows rapidly at the wall and is much larger. The

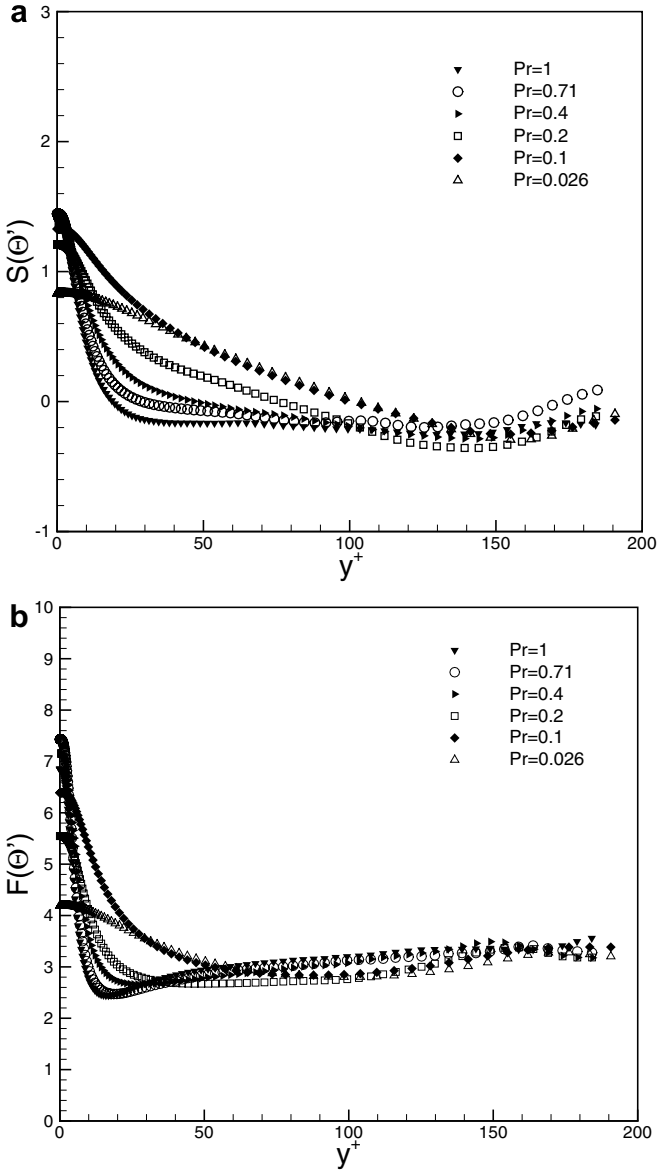

Fig. 11. (a) Skewness of temperature fluctuations and (b) flatness of temperature fluctuations.

intermittent behaviour of the wall region is thus more pronounced.

For $Pr = 0.71$, the present wall value ($S(\Theta') \simeq 1.4$) is slightly larger compared to Piller's result ($S(\Theta') \simeq 1.2$). However, the predicted behaviour of ($S(\Theta')$) for $Pr = 0.71$ is in general agreement with the one obtained in pipe by Piller (2005). The skewness of the temperature fluctuations at the wall, ($S(\Theta')$), is different from the skewness of the streamwise velocity fluctuations at the wall ($S(v_z') \simeq -0.25$, not shown here) owing to the different boundary conditions (the wall velocity equal to zero while the mixed-type boundary condition is used for the scalar). The non-zero value of $S(\Theta')$ in the near wall region indicates that the temperature fluctuations are asymmetric in this region. This confirms the intermittent character at the close vicinity of the wall, while the turbulence is nearly homogeneous far from the wall. The value of $S(\Theta')$ tends rapidly to the Gaussian value ($S(\Theta') = 0$) towards the pipe center.

Similar behaviour is observed for the radial distribution of the flatness factor $F(\Theta')$ of the temperature fluctuations. The flatness and skewness temperature fluctuations behave in quite similar manner: near the wall, a steep increase of $F(\Theta')$ is seen, identifying the existence of an intermittent region. Intermittency is more pronounced for Pr larger than $Pr = 0.026$, meaning that the probability of observing large variations from the mean temperature in the vicinity of the wall is much higher than in the center of the pipe, especially when the Prandtl number increases. For $Pr = 0.71$, $F(\Theta') = 7$ in the viscous wall region, which is slightly higher than Piller's prediction ($F(\Theta') = 5$) for a slightly smaller Re. Around $y^+ \simeq 20$, where $S(\Theta')$ is zero, the flatness $F(\Theta')$ presents a minimum value in accordance with Piller's finding. The value of this minimum increases with a decrease in Pr and disappears for $Pr \leqslant 0.2$. In the core region, $F(\Theta')$ exceeds 3. Unfortunately, no experimental or numerical data of the skewness and flatness factors at different Prandtl numbers for pipe flow as well as for channel flow are available in the literature for comparison purpose.

3.9. Nusselt number

Sleicher and Rouse (1975) proposed an empirical law for the effect of Prandtl number on Nusselt number, in a fully developped turbulent pipe flow. This law is applicable for $0.1 \leqslant Pr \leqslant 10^5$ and $10^4 \leqslant Re \leqslant 10^6$. Gnielinski (1976)

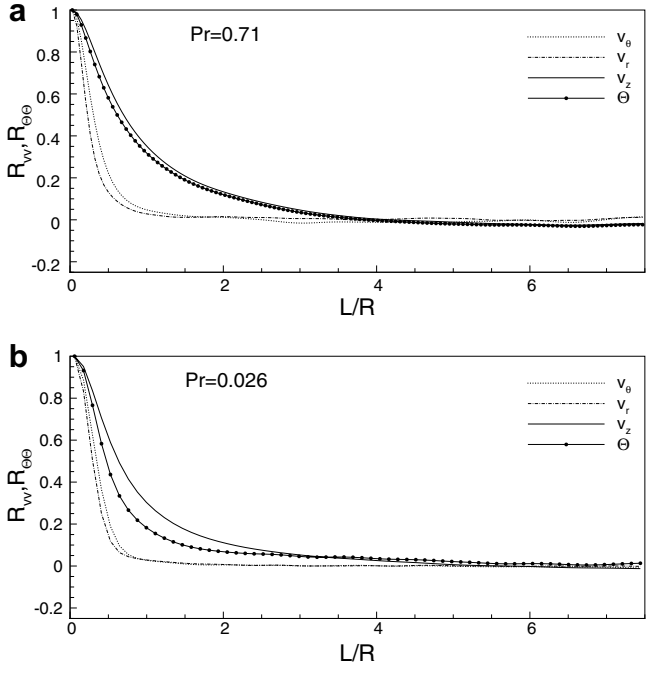

Fig. 12. Streamwise two-point correlations at $y^+ = 5$: (a) $Pr = 0.71$ and (b) $Pr = 0.026$.

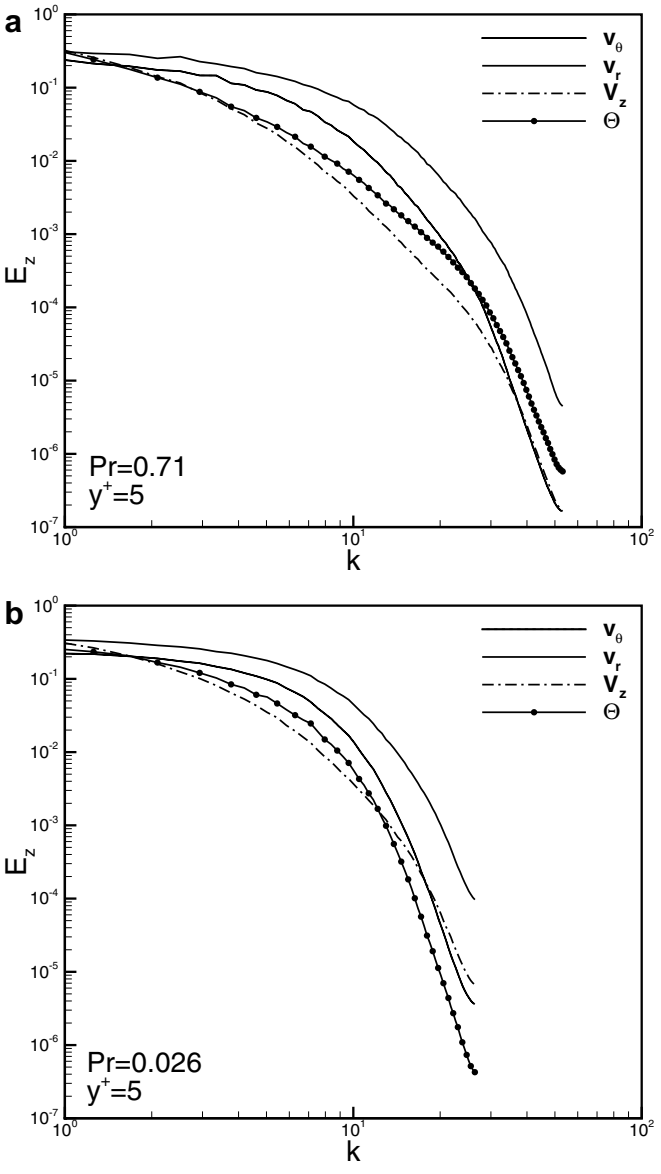

Fig. 13. Energy and temperature spectra at $y^+ = 5$: (a) $Pr = 0.71$ and (b) $Pr = 0.026$.

proposed constant property correlations for the friction coefficient and the Nusselt number valid for $2300 \leqslant Re \leqslant 5 \times 10^6$ and $Pr > 0.7$. Table 1 is prepared to show comparisons of the present Nusselt numbers, $Nu = hD/k$, for various Prandtl numbers at $Re = 5500$ ($Re_\tau = 186$). Also included are the simulations by Kawamura et al. (1998) (for a channel flow with constant heat flux at $Re_\tau = 180$). The agreement between the predicted Nusselt numbers and results of the literature is satisfactory, although the Reynolds number is smaller than the applicable range of the correlation given by Sleicher and Rouse (1975). It can be also seen that the present Nusselt number is slightly over-predicted in comparison with the correlation proposed by Gnielinski. However, the differences does not exceed the limits usually ascribed to the heat transfer coefficient in turbulent flows.

3.10. Two-point correlations

The streamwise two-point correlations of velocity and temperature fluctuations at $y^+ = 5$ are displayed in Fig. 12 for $Pr = 0.026$ and $Pr = 0.71$. For the axial velocity, the self-correlations $R_{v_z v_z}$ fall off to zero at a separation less than half the length of the computational domain (Fig. 12a and b), indicating that the length is sufficiently large to simulate adequately the largest eddies in the flow. The two-point correlations of the other two velocity components are characterized by a shorter length scale.

The streamwise two-point correlations of temperature fluctuations tend to zero at $y^+ = 5$ when the separation approaches half the pipe length, and the computational domain leads to adequate prediction of the temperature field. Since the results are not changed by increasing its length, the computational domain appears to be adequate to capture the largest thermal structures. The correlations of temperature fluctuations show an appreciable Prandlt number effect. These correlations extend to larger separations when Pr increases, suggesting that the effect of thermal structures become more prominent with increasing Pr, and essentially that the domain length used for the simulations with $Pr = 0.71$ is adequate for the simulations with smaller Prandtl numbers.

3.11. Energy and temperature spectra

The one-dimensional energy streamwise spectrum, defined as the Fourier transform of the corresponding self-correlation functions, is displayed in Fig. 13 at

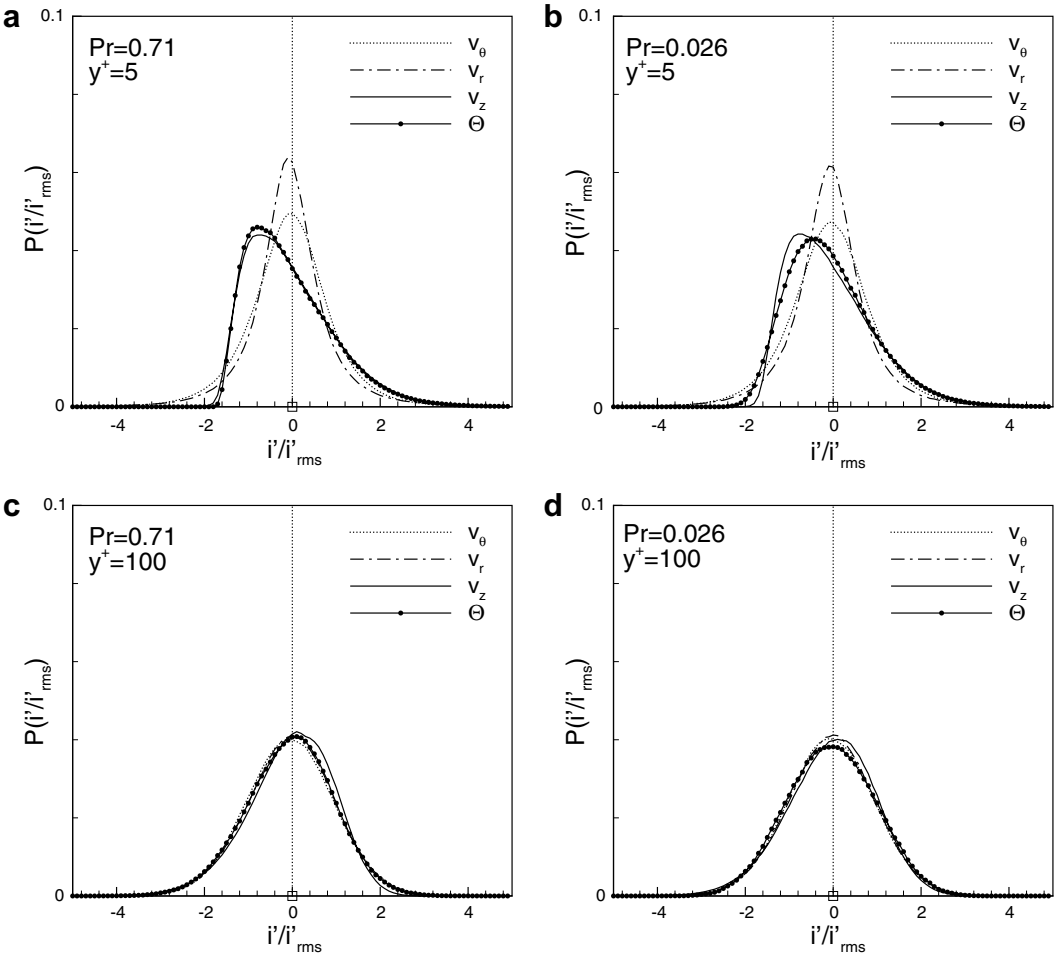

Fig. 14. Probability density function.

$y^+ = 5$. The spectra are normalized by their own mean-square values. The streamwise energy spectra indicate an adequate spatial resolution of the present simulations, since the spectra drop by several orders of magnitude. The energy spectra show a decrease in energy density when the wave number increases, and an absence of energy accumulation. For $Pr = 0.71$, the normalized spectra of the axial velocity component and temperature are nearly the same.

The streamwise spectrum of temperature at $y^+ = 5$ is shown in Fig. 13a and b for $Pr = 0.71$ and $Pr = 0.026$. We can note that the spectra still drop several orders of magnitude and thus the resolution is adequate. In the streamwise direction, the spectra increase significantly with increasing Pr at intermediate and high wave numbers, suggesting that the contribution of small and intermediate scales to the mean square value decreases in the near-wall region with decrease in Pr. Indeed, the small scales are gradually damped by the enhanced conductive effect with decreasing Pr (Abe et al., 2004).

3.12. Probability density function

In turbulent flows, probability density functions (pdfs) of velocity and scalar are fundamental in studying and modelling statistical characteristics of flow and heat transfer. The pdfs of streamwise, radial and azimuthal velocity components are depicted in Fig. 14, at different positions from the wall. In the vicinity of the wall (Fig. 14a), the distribution of the streamwise fluctuation v'_z deviates significantly from the Gaussian shape, denoting intermittency in flow. In the buffer region ($y^+ \simeq 14$), the skewness of v'_z tends to zero, indicating that the distribution of v'_z presents large positive fluctuations as much as large negative fluctuations, while the flatness of v'_z reaches its minimal value. That means that the largest streamwise velocity fluctuation amplitudes occur at $y^+ \simeq 14$, as one would expect from the predictions of the rms values of v'_z, shown in Fig. 3 (position of the maximal production of turbulent energy).

From the distance $y^+ \simeq 15$ and up to $y^+ \simeq 100$ (Fig. 14c), the pdfs shape of velocity components changes and approaches gradually a Gaussian distribution.

The pdfs of temperature fluctuations are also shown in Fig. 14a–d for two Prandtl numbers and two distances from the wall. Due to the significant similarity between the flow and the thermal field for $Pr = 0.71$, the distribution of temperature from the near-wall region ($y^+ = 5$) to the limiting edge of boundary layer, develop similarly to the distribution of streamwise velocity component. For

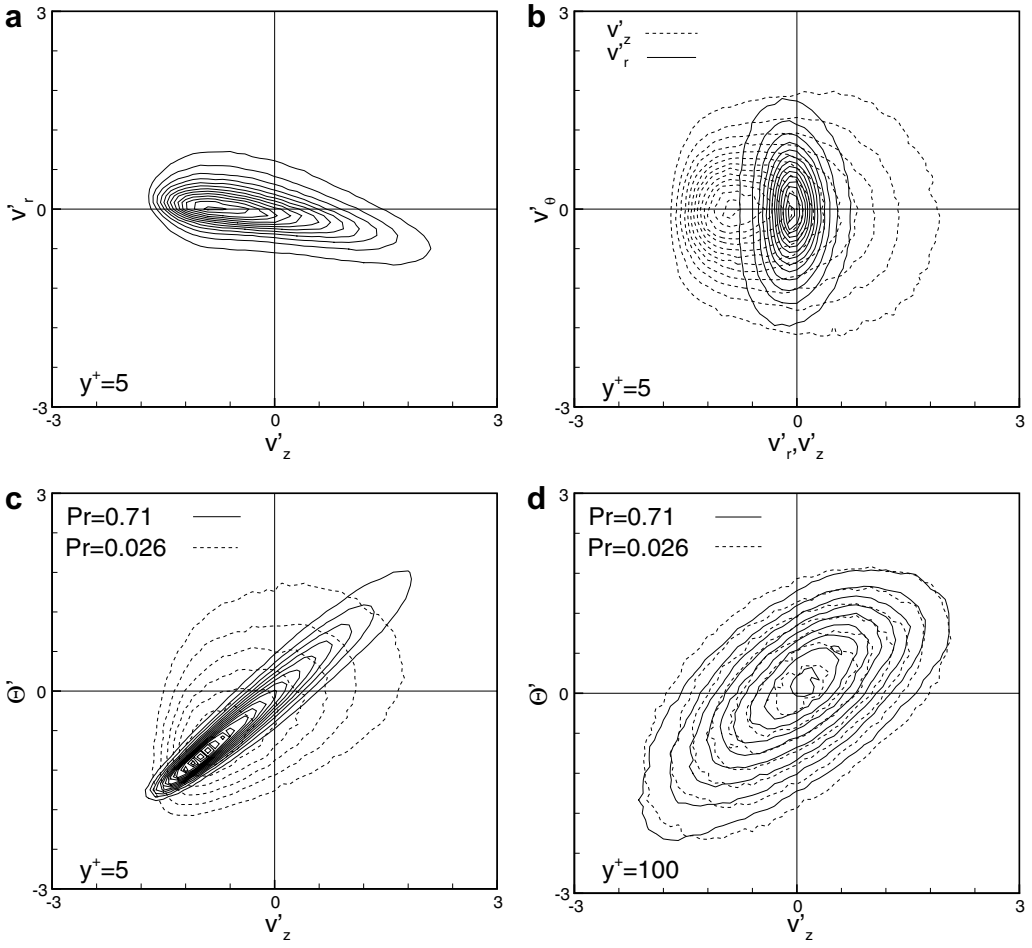

Fig. 15. Joint probability density function.

$y^+ < 18$, the most probable temperature are less than the mean temperature, while the opposite is found at $y^+ > 18$. Note that the pdf of v_z' is nearly symmetrical at $y^+ = 14$, while the pdf of temperature becomes symmetrical at larger values of y^+ ($y^+ = 18$). These predictions are in accordance with the experimental results of Antonia et al. (1988). At all distances from the wall, the Prandtl number effect is evident in the negative and positive tails of temperature pdfs. In the positive tails, the temperature pdfs show more and more larger values when Pr increases, suggesting that temperature distribution is more and more positively skewed. This trend is more pronounced when approaching the wall. In the negative tails, the temperature pdfs extend to larger negative values when Pr decreases.

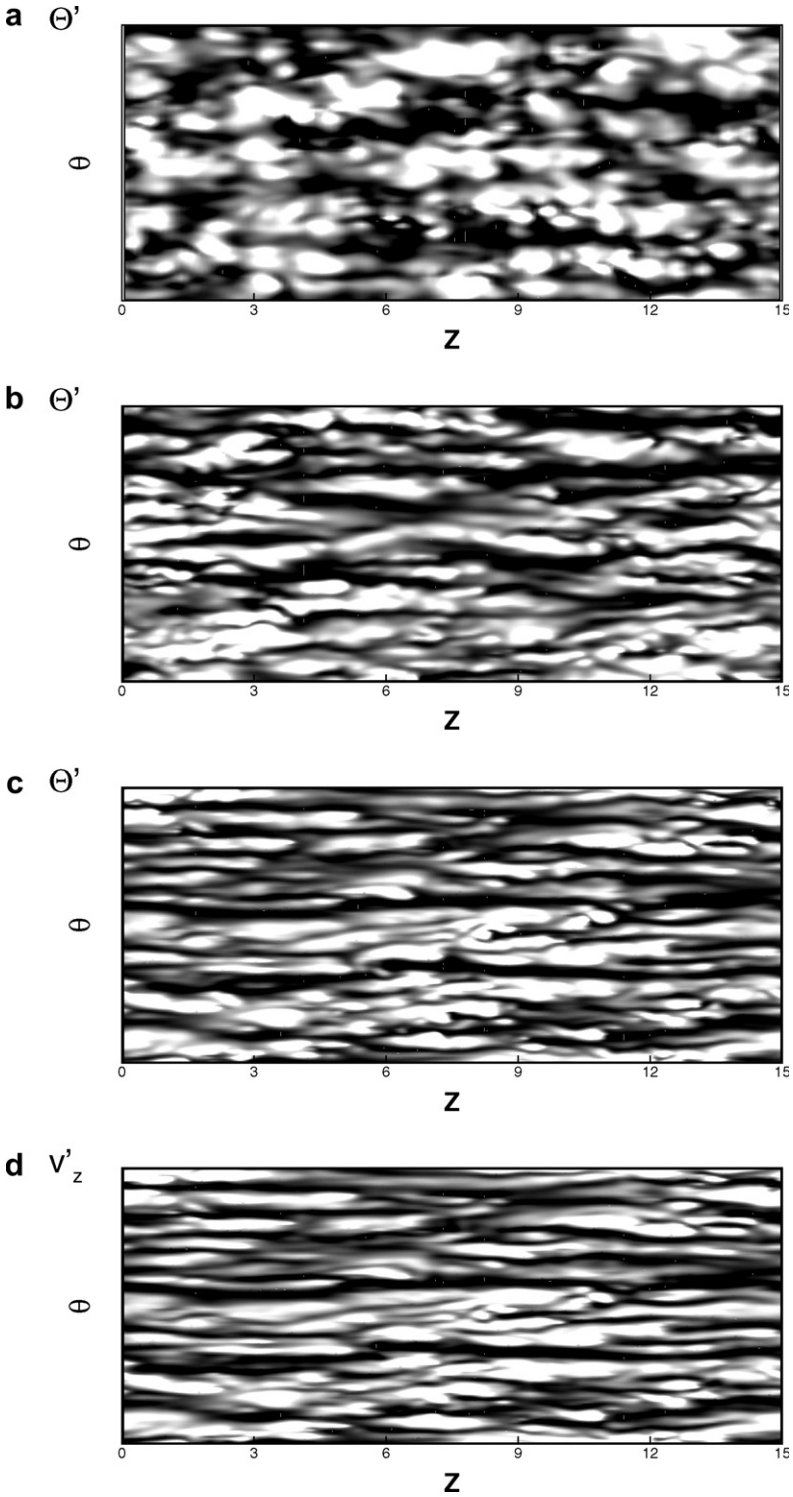

Fig. 16. Instantaneous temperature and velocity fluctuations at $y^+ \simeq 5$: (a) $Pr = 0.026$, (b) $Pr = 0.2$, (c) $Pr = 0.71$, and (d) $v_z'(Re = 5500)$.

3.13. Joint probability density function

The joint pdfs (jpdfs) are very useful to describe the physics of turbulent flows. The jpdfs at $y^+ = 5$ of the streamwise and radial velocity component, v'_z and v'_r, are given in Fig. 15a. The fluctuating quantities used for the joint pdfs are scaled with repect to the rms value. Fig. 15a demonstrates that ejections (second quadrant: $v'_z < 0$, $v'_r > 0$) and sweeps (fourth quadrant: $v'_z > 0$, $v'_r < 0$) have large contributions to the Reynolds shear stress $\langle v'_r v'_z \rangle$ and hence to the turbulent energy production. The joint pdfs in Fig. 15b show similar symmetries. Both correlations $\langle v'_r v'_\theta \rangle$ and $\langle v'_z v'_\theta \rangle$ have a symmetry around v_θ. This symmetry indicates that the Reynolds stresses $\langle v'_r v'_\theta \rangle$ and $\langle v'_z v'_\theta \rangle$ are zero. To better analyse the correlation between the flow and thermal fields, the joint pdfs between temperature and velocity component have been calculated at different distances from the wall (Fig. 15c and d). For $Pr = 0.71$, the predicted jpdfs denote a stronger correlation between temperature and v_z away from the wall. These trends support the DNS predictions by Hojin et al. (2000) in a turbulent boundary layer (in case of isoflux condition). Near the wall, the correlation is weaker when Pr decreases (Fig. 15c) indicating that temperature is less well correlated with v_z when decreasing Pr, because of the strong conductive effects. Moreover, a decrease in Pr leads to a decrease in the correlations at higher magnitude fluctuations. As the core region is approached, the difference between the jdpfs (Θ', v'_z) at $Pr = 0.71$ and at $Pr = 0.026$ practically disappears (Fig. 15d). The maximum which was localised in the third quadrant is now close to the origin. The contributions to $\langle v'_z \Theta' \rangle$ are more significant in the first and third quadrants for both Prandtl numbers. This reflects the results of the positive value in $\langle v'_z \Theta' \rangle$, as shown in Fig. 7.

3.14. Instantaneous flow and temperature fields

To explore the effects of the Prandtl number on the thermal structures, instantaneous temperature and streamwise velocity fluctuations are visualized in Fig. 16. Note that the velocity fields are the same for the various Prandtl numbers since the temperature behaves as a passive scalar. In the case of a low Prandtl number ($Pr = 0.026$), a regular distribution of the temperature fluctuations is observed. A visualization of the temperature fields in a (r, θ)-plane (not shown here) reveals a rather uniform distribution of the thermal field, denoting a large width of the conductive sublayer. For $Pr = 0.2$, streaky structures are observed in the temperature fluctuations (Fig. 16b). The conductive region becomes thinner leading to a reduction of the molecular heat flux and an enhancement of the turbulent heat flux normal to the wall. These trends are more pronounced for higher Prandtl numbers.

In the case of $Pr \simeq 1$, a similarity between the velocity and thermal streaky structures is observed. However, the similarity between temperature (Fig. 16c) and streamwise velocity (Fig. 16d) is expected to be better in the case of isothermal wall (as compared to the isoflux-wall case). Fig. 16c and d clearly exhibits that the fluid temperatures are correlated with the fluid speeds. These predictions are in accordance with the DNS results obtained by Hojin et al. (2000) in a turbulent thermal boundary layer.

4. Conclusion

In the present work, DNS of turbulent heat transfer pipe flow under isoflux conditions have been performed at low Reynolds number ($Re = 5500$) and various Prandtl numbers. Different statistical turbulence quantities including the mean and fluctuating temperatures, the heat transfer coefficients and the turbulent heat fluxes are obtained and analyzed. An effort to reveal the Prandtl number effects on turbulent heat transfer is sketched. The validation of the present approach (DNS) has been achieved by comparing our predictions with some available results of the literature. The present results are in reasonably good agreement with the findings of the literature: the rms of temperature fluctuations and turbulent heat fluxes are increased when increasing the Prandtl number. Their near-wall behaviours are accurately predicted. The Nusselt number is in satisfactory agreement with the correlation by Sleicher and Rouse (1975) and in fair agreement with the numerical predictions of Kawamura et al. (1998) and Piller (2005). At all distance $y^+ < 18$, the most probable temperature is less than the mean temperature, while the opposite is found at $y^+ > 18$. Near the wall, the correlation between Θ' and v'_z is weaker when Pr decreases, because of the strong conductive effects. As the core region is approached, the differences between the jdpfs (v'_z, Θ') for $Pr = 0.026$ and $Pr = 0.71$ are very small. Visualizations of the intantaneaous temperature and velocity fields exhibit streaky structures and show that temperature and streamwise velocity fluctuations are highly correlated for $Pr \simeq 1$. The streaky structures in the temperature fluctuations are more pronounced for the highest Prandtl numbers considered in this work. One objective of this research was also to explore the curvature effects on turbulent heat transfer in duct flows, by comparing our DNS predictions for axisymmetric pipe flow to the findings for plane channel flow. There are only slightly differences between the turbulence statistics of the two flow configurations. The wall curvature is seen to slightly enhance the temperature fluctuations. This indicate that, irrespective of Pr, the wall curvature does not have a major impact on turbulent heat transfer. An other interesting outcome of the present DNS is to establish databases of various turbulence statistics of turbulent transport phenomena at different Prandtl numbers ($Pr \leqslant 1$). These databases will be undoubdtedly helpful for evaluating and developing turbulence models (for example improving the empirical laws used in classical models of turbulence), and especially for describing heat transfer in turbulent pipe flow with $Pr \leqslant 1$.

Acknowledgments

The support of this work by IDRIS under Grant 051265 is greatly acknowledged. The authors also thank the editor and referees for their useful suggestions.

References

Abe, H., Kawamura, H., Matsuo, Y., 2004. Surface heat-flux fluctuations in a turbulent channel flow up to $Re_\tau = 1020$ with $Pr = 0.025$ and 0.71. Int. J. Heat Fluid Flow 25, 404–419.

Antonia, R.A., Krishnamoorthy, L.V., Fulachier, L., 1988. Correlation between the longitudinal velocity fluctuation and temperature fluctuation in the near-wall region of a turbulent boundary layer. Int. J. Heat Mass Transfer 31 (4), 723–730.

Bremhorst, K., Bullock, K.J., 1973. Spectral measurements of turbulent heat and momentum transfer in fully developed pipe flow. Int. J. Heat Mass Transfer 16, 2141–2154.

Chapman, D.R., Kuhn, G.D., 1986. The limiting behaviour of turbulence near the wall. J. Fluid Mech. 70, 265–1986.

Eggels, J.G.M., Unger, F., Weiss, M.H., Westerweel, J., Adrian, R.J., Friedrich, R., Nieuwstadt, F.T.M., 1994. Fully developed turbulent pipe flow: a comparison between Direct numerical simulation and experiment. J. Fluid Mech. 268, 175–209.

Feiz, A.A., Ould-Rouis, M., Lauriat, G., 2005. Turbulence statistics in a fully developed rotating pipe flow. Int. J. Enhanced Heat Transfer 12 (3), 273–288.

Gnielinski, V., 1976. Neue gleichungen für den wärme- und den stoff übergang in turbulent durchströmenten rohren und kanalen. Int. Chem. Eng. 16, 359.

Gowen, R.A., Smith, J.W., 1967. The effect of the Prandtl number on temperature profiles for heat transfer in turbulent pie flow. Chem. Eng. Sci. 22, 1701–1711.

Hishida, M., Nagano, Y., Tagawa, M., 1986. Transport process of heat and momentum in the wall region of tubulent pipe flow. In: Tien, C.L. et al. (Eds.), Proceedings of the 8th International Heat Transfer Conference. Hemisphere Publishing Corp. 3, Washington, DC, pp. 925–930.

Hojin, K., Choi, H., Lee, J.S., 2000. Direct numerical simulation of turbulent thermal boundary layer. Phys. Fluids 12 (10), 2555–2568.

Kader, B.A., 1981. Temperature and concentration profiles in fully turbulent boundary layers. Int. J. Heat Mass Transfer 24 (9), 1541–1544.

Kawamura, H., Ohsaka, K., Abe, H., Yamamoto, K., 1998. DNS of turbulent heat transfer in channel flow with low to medium-high Prandtl number fluid. Int. J. Heat Fluid Flow (19), 482–491.

Kawamura, H., Abe, H., Matsuo, Y., 1999. DNS of turbulent heat transfer in channel flow with respect to Reynold and Prandtl number effects. Int. J. Heat Fluid Flow (20), 196–207.

Kays, W.M., Perkins, H.C., 1973. In: Rohsenow, W.M., Harnett, J.P. (Eds.), Handbook of Heat Transfer. McGraw-Hill, New York (Section 7).

Martinelli, R.C., 1947. Heat transfer to molton metals. Trans. ASME 69, 947.

Montreuil, E., 2000. Simulation numérique pour l'aérothermique avec des modèles de sous-mailles, Ph.D. Thesis, Université Pierre et Marie Currie, France.

Musschenga, E.E., Hamersma, P.J., Fortuin, J.M.H., 1992. Momentum, heat and mass transfer in turbulent pipe flow: the extended random surface renewal model. Chem. Eng. Sci. 47 (17), 4373–4392.

Myong, H.K., Kasagi, N., Hirata, M., 1989. Numerical prediction of turbulent pipe flow: heat transfer for various Prandtl number fluids with the improved $k - \epsilon$ turbulence model. JSME Int. J. 32, 613–622.

Na, Y., Hanratty, T.J., 2000. Limiting behavior of turbulent scalar transport close to the wall. J. Heat Mass Transfer 43, 1749–1758.

Petukhov, B.S., 1970. Heat transfer and friction in turbulent pipe flow with variable physical properties. Adv. Heat Transfer 6, 503–504.

Piller, M., 2005. Direct numerical simulation of turbulent forced convection in a pipe. Int. J. Numer. Meth. Fluids 49, 583–602.

Satake, S., Kunugi, T., 2002. Direct numerical simulation of turbulent heat transfer in an axially rotating pipe: Reynold stress and scalar-flux budgets. Int. J. Numer. Method. Heat Fluid Flow 12 (8), 985–1008.

Sleicher, C., Rouse, M.W., 1975. A convenient correlation for heat transfer to constant and variable property fluids in turbulent pipe flow. Int. J. Heat Mass Transfer 18, 667–683.

Takagi, T., Hirai, S.H., 1998. Turbulent transport of momentum and scalar in swirling flows with and without combustion. Int. J. Fluid Mech. Res. 25 (1–3), 1–13.

Tennekes, H., Lumley, J.L., 1972. A First Course in Turbulence. MIT Press Design Department, Cambridge, MA.

Thakre, S.S., Joshi, J.B., 2000. CFD modeling of heat transfer in turbulent pipe flows. AIChe J. 46 (9), 1798–1812.

Tricoli, V., 1999. Heat transfer in turbulent pipe flow revisited: similarity law for heat and momentum transport in low-Prandtl-number fluids. Int. J. Heat Mass Transfer 42, 1535–1540.

Von Karman, T., 1939. The analogy between fluid friction and heat transfer. Trans. ASME 61, 705.

Yakhot, V., Orszag, S.A., Yakhot, A., 1987. Heat transfer in turbulent flows – I. Pipe flow. Int. J. Heat Mass Transfer 30 (1), 15–22.